Observation of cosmic-ray anisotropy in the decade below 1 PeV with a pentagon array

S. Mortazavi Moghaddam[1,2] and M. Bahmanabadi[1,3,*]

[1]ALBORZ Observatory, Sharif University of Technology, P.O.Box 11155-9161 Tehran, Iran
[2]Department of Physics, Semnan University, P.O.Box 35131-19111 Semnan, Iran
[3]Department of Physics, Sharif University of Technology, P.O.Box 11155-9161 Tehran, Iran

(Received 7 February 2018; published 13 March 2018)

The study of the anisotropy of the arrival directions is an essential tool to investigate the origin and propagation of cosmic rays primaries. A pentagon array has been designed to collect data around the knee region of cosmic ray spectrum. The experimental results of this array obtained from October 2016 to October 2017. During this period, more than 5.3×10^5 extensive air shower events at energies in the decade below 1 PeV has been accumulated by this array at Sharif University of Technology in Tehran (35°43′N, 51°20′E, 1200m a.s.l $= 890$ g cm^{-2}). In analyzing the data set, we have used appropriate techniques of analysis and considered environmental effects. We report the analysis of the sidereal anisotropy of Galactic cosmic rays (GCRs). In this analysis, in addition to the Compton- Getting effect due to the motion of the earth in the Galaxy, an anisotropy has been observed which is due to a unidirectional anisotropy of cosmic ray flow along the Galactic arms.

DOI: 10.1103/PhysRevD.97.062001

I. INTRODUCTION

Although cosmic rays have been known for nearly a century, their sources are still not well known. This is mainly due to the fact that their paths in the galactic magnetic field are bent and they do not individually point back to their sources. Cosmic rays in the lower energy range have gyro radii of about 1 pc or less in typical galactic magnetic fields (a proton with an energy of 10^{15} eV would have a gyro radius of 1 pc in a 1 μG field). Moreover, since these magnetic fields are chaotic on scales ranging at least from 10^8 cm to 10^{20} cm [1], the transport of charged cosmic rays is diffusive up to high energies, so the angular distribution in their arrival direction when they reach the Earth is isotropic [2]. Therefore, even collectively, the cosmic ray arrival directions hold virtually no information about the source distribution in space. However, as the energy of the cosmic ray increases, it can appear either because the diffusive approximation does not hold anymore, or because the diffusion coefficient becomes large enough to reveal intrinsic inhomogeneities in the source distribution. Specifically, even if the diffusive regime holds, the density of cosmic ray sources in the Galaxy is believed to be larger in the inner regions than in the outer ones, and this can cause a slightly higher cosmic ray flux coming from the Galactic center than from the anticenter. Meanwhile, the global cosmic ray streaming away from the Galactic plane (toward the halo) can be a source of measurable anisotropy. However, the detailed angular distribution of cosmic rays is quite hard to predict, even if we assume a definite source distribution, because it also depends on the propagation conditions, which are related to both large scale and small scale magnetic field configurations, and on the position of the Earth relative to major magnetic structures, such as the local Galactic arm.

From a general point of view, the anisotropy characteristic of cosmic rays provides useful information to constrain the Galactic cosmic ray diffusion models, especially the effective diffusion coefficients, related to the magnetic field structure. Indeed the level of cosmic ray anisotropy depends on the diffusion coefficient, D. In a simple model where cosmic ray sources uniformly distributed through the disk with a total thickness $2h$ and the cosmic rays are confined in a halo of height H, the anisotropy at distance z from the central galactic plane($|z| < h$) is estimated as $\delta_z \simeq 3D/cH \times z/h$ [3]. With assumption that $z/h = 0.1$ ($z = 20$ pc, $h = 200$ pc), the expected value of the anisotropy at energy 10^{14} eV, $\delta_z(10^{14}\ \text{eV})$, is typically below 1% and can be as low as 0.03% [4]. Anisotropy measurements at various energies can thus provide crucial information about the energy dependence of the diffusion coefficient. This information is particularly important to constrain the Galactic cosmic ray source spectrum, since it sets the relation between the source power law index and the observed one, through the energy dependent confinement of cosmic rays in the Galaxy. This diffusion maybe is broadly along the magnetic field lines which are in tubes of dimensions greater than the gyro radii. So the direction of

*bahmanabadi@sina.sharif.edu

the peak of the anisotropy would indicate the direction back towards the cosmic ray source, and the amplitude of the anisotropy would give information on the scattering process involved in the diffusion. Specifically, an estimate of the mean free path might be obtained.

The anisotropy is due to a combination of effects. An apparent anisotropy in the intensity of particles is related to Earth's motion relative to the rest frame of the cosmic ray plasma, which is called Compton- Getting effect [5]. This effect causess an energy independent dipole anisotropy with maximum in the direction of relative motion. The earth's rapid motion in space, resulting from the rotation of our galaxy, results variations in cosmic ray intensity fore and aft of the earth's motion. The expected anisotropy amplitude due to the Compton-Getting effect can be expressed as

$$\delta_{CG} = (\gamma + 2)\frac{u}{c}\cos\beta. \tag{1}$$

Where γ denotes the power law index of the energy spectrum of cosmic rays, u the velocity of the detector relative to the production frame of the cosmic rays (where they are presumed to be isotropic), c the speed of light, and β the cosmic ray direction relative to u, i.e., $\cos\beta$ is the projection of the cosmic ray along the forward direction of u. In fact the value of $(\gamma+2)\frac{u}{c}$ is $(f_{\max}-f_{\min})/(f_{\max}+f_{\min})$ with $f_{\max}$ the counting rate along the direction of the velocity and $f_{\min}$ along the contrary direction. The magnitude of the anisotropy is extremely small and independent of the cosmic ray energy. Our data will be analyzed in a sun-centered frame, and so if data accumulation is done over an integer number of solar years, it is only necessary that the orbital speed of the Earth around the sun ($\sim$30 km s^{-1}) be considered. The large effect due to the Galactic rotational speed (220 km s^{-1}) will cancel out as the data are averaged over this time(assuming uniform data-taking over this period of time) [6]. Many experiments have been carried out for detection of this effect [6,7].

Studies of Doppler effect on globular clusters and extra galactic nebulae have revealed that the Earth's motion is about 220 km s^{-1} towards right ascension $\alpha \simeq 21$ h and declination $\delta \simeq 47°$N due mainly to the rotation of the Galaxy. This motion, with a speed of about 0.1% c will affect the intensity of the incoming cosmic rays by changing both the energy of the cosmic ray particles and the number received per second. Using value of 220 km s^{-1} for u, and 2.7 for the spectral index, Eq. (1) gives a Compton-Getting effect (CGE) amplitude of $(\gamma+2)\frac{u}{c} = 0.345\times10^{-2}$ for the fractional forward-backward asymmetry caused by the motion of the earth in the Galaxy.

Other effects that can produce sidereal modulation is solar diurnal and seasonal changes in the atmospheric temperature and pressure. As the atmospheric temperature and pressure change during the course of a day, the balance of cosmic ray secondary particle interaction and decay changes. This propagates to changes in the detection rate that depend on the detector type (air shower, underground muon, surface muon) and on the energy threshold. These changes tend to have a strong Fourier component with a frequency of one solar day ($\simeq$365 cycles/year) and one solar year (1 cycle/year). In some (but by no means all) experiments, the interplay between the daily and seasonal modulation can produce significant modulation in sideband frequencies of $\simeq(365\pm1)$ cycles/year [8]. The modulation with frequency 366 cycles/year appears as a sidereal modulation. The magnitude of the atmospheric contribution to apparent sidereal anisotropy can be estimated from the amplitude of the antisidereal (364 cycles/year) frequency. If it is large, the atmospheric effect can be subtracted using the amplitude and phase of the antisidereal component. The anisotropy that remains after accounting for the Compton- Getting and atmospheric effects is due to solar and galactic effects. At the lowest energies ($\sim$100 GeV), the interplanetary magnetic field (IMF) produced by the solar wind effects the sidereal anisotropy: when the local IMF points toward the sun, the anisotropy peaks at about 18 h right ascension, while it peaks at 6 h when it points away [9,10]. The average over the two configurations produces a small, residual anisotropy peaking at around 2–4 h. At higher energies, local IMF plays a negligible role. Instead, the heliosphere extending to distances of order 100 AU is believed to induce anisotropy in cosmic rays with energies around 1 TeV [11,12]. Beyond this energy, the anisotropy is believed to be primarily of galactic origin. For instance, the galactic magnetic field around the solar system neighborhood could produce anisotropy. Also, an uneven distribution of sources of cosmic rays (presumably, mostly supernova remnants) may produce anisotropy. It is believed that star formation(and thus, supernova remnants) occur primarily in the spiral arms of the galaxy. The earth is located at the inner edge of the Orion spur. Thus, in the direction of the Orion spur(galactic longitude between 60° to 270°) they are distributed nearby sources of cosmic rays, while in the complementary direction, they are much further away.

Due to the small anisotropy, it is necessary to have a large data set of measurements to cover the uncertainties of the counting measurements. A simple method for recording many cosmic rays is to record coincidences between a number of detectors. Few statistically significant anisotropies have been reported from extensive air shower experiments in the three last decades. Analysing the Akeno experiment, Kifune *et al.* (1986) [13] reported results of about 2×10^{-3} at about 5 to 10 PeV. Aglietta *et al.* (1996,EAS-TOP) [14] published an amplitude of $(3.7\pm0.6)\times10^{-4}$ and phase $\phi = (1.8\pm0.5)$ h local sidereal time (LST), at $E_0 \approx 200$ TeV. An overview of experimental results can be found in [15].

We have operated a pentagon array on the roof of the restaurant building at Sharif University of Technology in

Tehran(35°43′N, 51°20′E, 1200m a.s.l = 890 g cm^{-2}). This paper reveals results of the array after one year data acquisition with more than 5.3×10^5 EAS events and zenith angles ≤45° at energies in the decade below 1 PeV. The main purpose of this article is to study the arrival direction of EAS events and study of anisotropy, and in particular the unidirectional anisotropy of cosmic rays flow along the Galactic arms which was observed in the sidereal time at energies in the decade below 1 PeV. We describe the experimental setup in Sec. II, and the data analysis and discussion in the next sections.

II. EXPERIMENTAL SET UP

Figure 1 shows an array including 5 plastic scintillation detectors (each one $50 \times 50 \times 2$ cm^3) are placed at the corners of a pentagon with side length 5m. Each detector is housed in a galvanized iron pyramidal light enclosure with height of 20 cm and a photomultiplier tube (PMT, 9813B) is installed at the apex of the light enclosure. The size of the detectors and height of light enclosure had been optimized previously [16]. The detectors are numbered from 1 to 5 and the time lags of particles passing through the detectors No. 2, 3, 4, and 5 with the detector No. 1 are recorded. The electronic circuit shown in Fig. 1, for recording extensive air showers has been used. Signals from the PMTs are connected to an 8-channel fast discriminator (CAEN N413A) which was operated in fixed level of -200 mV. The output of the discriminator channel related to the detector No.1 has been sent to the start inputs of 4 time to amplitude converters (TAC, ORTEC566) and the output of the other channels of the discriminator related to the 4 other detectors have been sent to the stop inputs of the same TACs by external delay cables. Finally the outputs of the

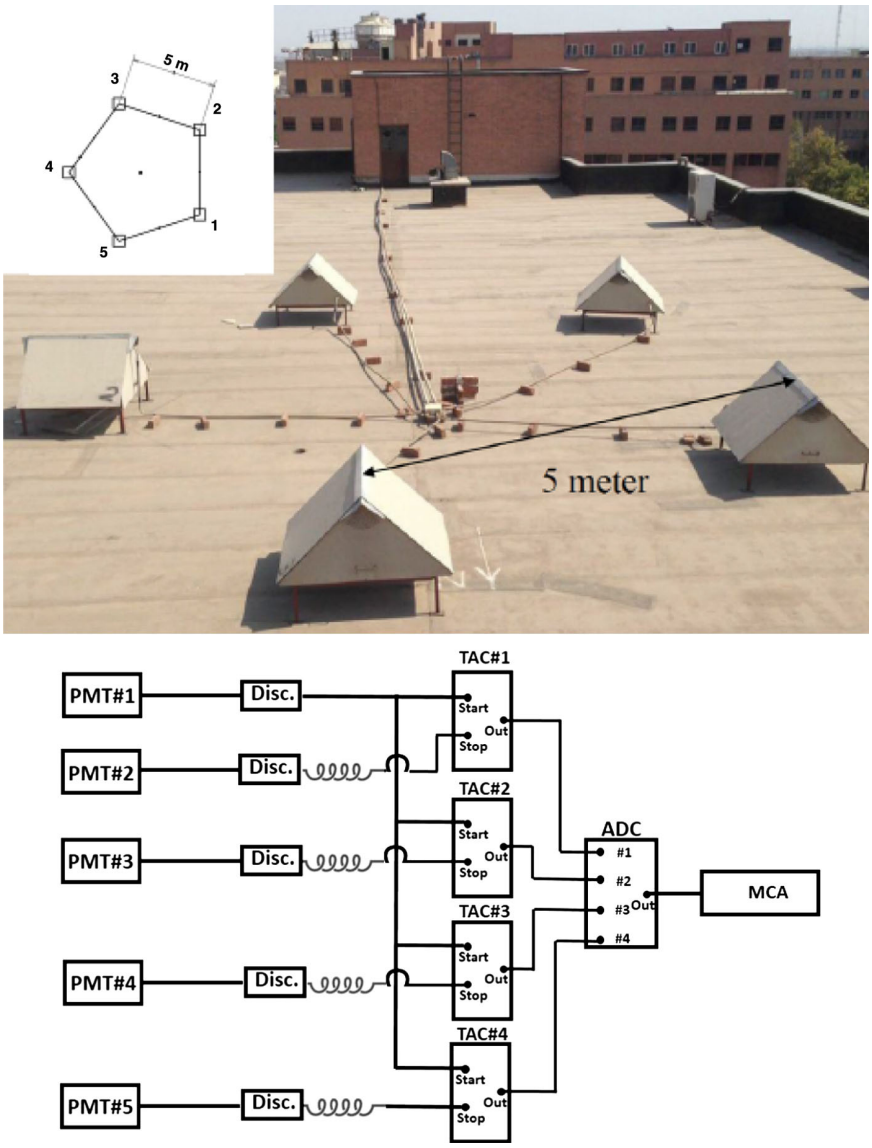

FIG. 1. Pentagon array configuration, and schematic view of the electronic circuit.

TACs, which were set to a full scale of 200 ns, are fed into a multichannel analyzer (MCA) via an analog to digital converter (ADC, KIAN AFROUZ Inc.) unit. In the electronic circuit, the output signal of the coincidence between the detectors No. 1 and No. 2 is a signal gate for recording an EAS. An another condition to record an EAS event is coincidences between the detector No. 1 and the other detectors (No. 2 to No. 5) in a time width about 50 ns.

III. ANALYSIS AND DISCUSSION OF DATA

A. Event rate and atmospheric effect on counting rate

The present data set from the pentagon array covers a one-year period from October 2016 to October 2017. During this time, 532794 EAS events with zenith angles $\leq 45°$ at energies in the decade below 1 PeV, have been collected, so that the data recording is 1 event per ≈ 34.6 seconds. The time-spacing distribution of successive events is demonstrated in Fig. 2. Since events occur randomly in time, it is expected that its distribution follows an exponential function as $f(t) = f(0)e^{-t/\tau}$. The event rate can be obtained by fitting the function $f(t)$ on the events time-spacing distribution. One event per $\tau = (34.5 \pm 0.1)$ s is also obtained using the fit function $f(t)$. The fitting of this function is performed without the first point (the 5s point), since the low value of this point may be the result of a dead time. Deviation from the exponential law indicates a non-random component for the cosmic ray flux. Bhat *et al.* [17] reported a significant deviation from the exponential law, but subsequent investigations failed to confirm this result. Our observed distribution is also in good agreement with the exponential law.

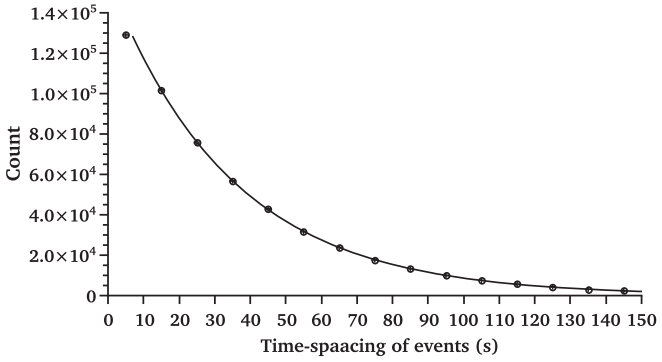

FIG. 2. Time-spacing distribution of successive EAS events.

The event rate depends on a number of parameters, which the premier of them are atmospheric pressure and temperature. The variation of the EAS event rate can be caused by two main atmospheric parameters: (1) atmospheric pressure, and (2) atmospheric temperature [18]. Synoptic meteorological data was taken from the Mehrabad weather station. The EAS counts dependence on barometric pressure and ground-level temperature in 3-h intervals, over zenith angles $\leq 45°$ and all azimuthal angles are shown in Fig. 3. In order to remove these pressure and temperature dependences, we use the following method.

We assume that the event rate is detachable into a function of barometric pressure and a function of the ground-level temperature. These relationships are modeled by two exponential equations: $R_P = R_{0P}e^{-\beta_1(P-P_0)}$, and $R_T = R_{0T}e^{-\beta_2(T-T_0)}$, where R_P and R_T are EAS events rate corresponding barometric pressure (P), and ground-level temperature (T), respectively [19]. In this analysis the barometric pressure coefficient (β_1), and temperature coefficient (β_2) can be introduced as the proportionality constants of the relation $\frac{dR_P}{R_P} \propto -dP$, and $\frac{dR_T}{R_T} \propto -dT$ respectively. Assuming that these effects are detachable, we first correct the event rate for one parameter (for example, pressure), and then we make another suitable correction for other parameter (in this case temperature).

(1) In the first step we correct the event rate for barometric pressure (P) as follow: The values of $R_{0P} = \frac{1}{N}\sum_{i=1}^{N} R_i$, and $P_0 = \frac{1}{N}\sum_{i=1}^{N} P_i$, are obtained, where $N = 1708$, which is the number of 3-h intervals in the experimental data, R_i and P_i are

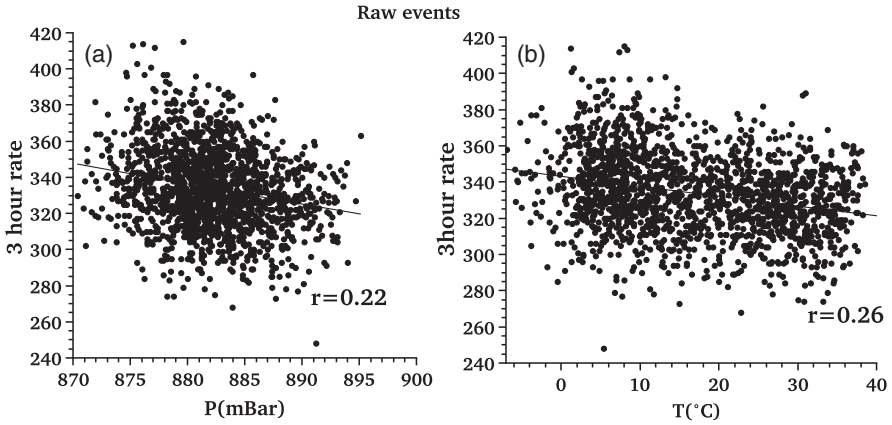

FIG. 3. uncorrected 3-h counts as a function of the ambient pressure (a), and ambient temperature (b). The black lines represent the exponential fitted functions.

the recorded count rate and pressure respectively in ith 3-h interval. The proportionality constant(β_1) can be calculated by least-square method as,

$$\beta_1 = -\frac{\sum_{i=1}^{N}(P_i - P_0)(\ln R_i - \ln R_{0P})}{\sum_{i=1}^{N}(P_i - P_0)^2}. \quad (2)$$

Considering the linear correlation between two variables $\ln R_P$, and P, the correlation coefficient, r, is defined as follows,

$$r = -\frac{\sum_{i=1}^{N}(P_i - P_0)(\ln R_i - \ln R_{0P})}{\sqrt{\sum_{i=1}^{N}(\ln R_i - \ln R_{0P})^2}\sqrt{\sum_{i=1}^{N}(P_i - P_0)^2}}. \quad (3)$$

With taking $\sigma_R^2 = \frac{1}{N}\sum_{i=1}^{N}(\ln R_i - \ln R_{0P})^2$, and $\sigma_P^2 = \frac{1}{N}\sum_{i=1}^{N}(P_i - P_0)^2$, Eq. (2) can be written as $\beta_1 = r\frac{\sigma_R}{\sigma_P}$, and $\Delta\beta_1 = \pm\beta_1 \frac{1}{r}(\frac{1-r^2}{N-3})^{\frac{1}{2}}$. The values of $R_{0P} \simeq 334$ per 3 h, $P_0 \simeq 882$ mb were obtained from the data set. There is a $r \simeq 0.22$ correlation coefficient between atmospheric pressure and EAS events rate in this experimental period [Fig. 3(a)]. The barometric coefficient value, β_1, for this period is $\simeq(3.0 \pm 0.3) \times 10^{-3}$/mb. This value of β_1 was used to correct the events rate for pressure using $R_P = R_{0P}e^{-\beta_1(P-P_0)}$, where R_P shows the expected value for events rate in the measured atmospheric pressure, P. Hence, the pressure corrected events, $R_P^{\rm cor}$, is obtained as $R_P^{\rm cor} = \frac{R_{\rm meas}}{R_P^{\rm exp}}R_{0P}$, where $R_{\rm meas}$ and $R_{\rm exp}$ are the measured events rate in the data acquisition, and the expected events rate by the equation $R_P^{\rm exp} = R_{0P}e^{-\beta_1(P-P_0)}$, respectively.

Figure 4(a) shows pressure corrected EAS counts as a function of atmospheric pressures. As presented in Fig. 4(a), the correlation coefficient was dropped from $r = 0.22$ to $r = 3.82 \times 10^{-5}$, indicating that this method can adequately correct the array data for atmospheric pressure.

(2) In the second step the event rate is corrected for ground-level temperatue just like the first step, with the following transformations:
   (a) $R_{0P} \to R_{0T}$, with $R_{0T} = \frac{1}{N}\sum_{i=1}^{N} R_P^{\rm cor} \simeq 334$ per 3 h,
   (b) $P_0 \to T_0$, with $T_0 = \frac{1}{N}\sum_{i=1}^{N} T_i = 16.7°$C,
   (c) $R_i \to R_P^{\rm cor}$, and $P_i \to T_i$.

With these transformations, the final corrected event rate for pressure and temperature, $R_{\rm cor}(P,T)$, is obtained as $R_{\rm cor}(P,T) = \frac{R_P^{\rm cor}}{R_T^{\rm exp}}R_{0T}$. Where the expected events rate, $R_T^{\rm exp}$, is calculated by the equation $R_T^{\rm exp} = R_{0T}e^{-\beta_2(T-T_0)}$, with $\beta_2 \simeq (2.0 \pm 0.1) \times 10^{-3}/°$C. Figure 4(b) shows $R_{\rm cor}(P,T)$ as a function of atmospheric temperature. Finally after these corrections, the correlation coefficient is $r = -0.008$.

B. Zenith angle distribution of the EAS events

With arrangement of the pentagon array (Fig. 1), arrival direction of an air shower can be determined by the least-square method [20], using time lag between the detector No. 1 and the other detectors. In this method is assumed the shower direction is the normal to the propagating shower front, which is approximately a plane surface in the proximity of the shower axis. Because of the walls around the array location, only zenith angles less than 45° is consider. Figure 5 shows zenith angle distribution of showers. This feature can be understood since at large angles, showers tend to decay before they reach the ground and consequently the zenith angular distribution per solid angle of showers can be represented by the relation $N(\theta) = N(0)\cos^n\theta$. With this relation, $n = 7.2 \pm 0.1$ is obtained from the pentagon array data with a regression 0.999 which is consistent with our simulation results [21].

C. The sensitive energy range in the pentagon array

Since we can not determine the energy of the showers on an event-by-event basis, we estimate the energy range of our array by the CORSIKA code for simulation of EAS events [22]. In order to record a shower it is necessary at least one particle passes through each of the five detectors. The trigger probability of a ground based array depends on

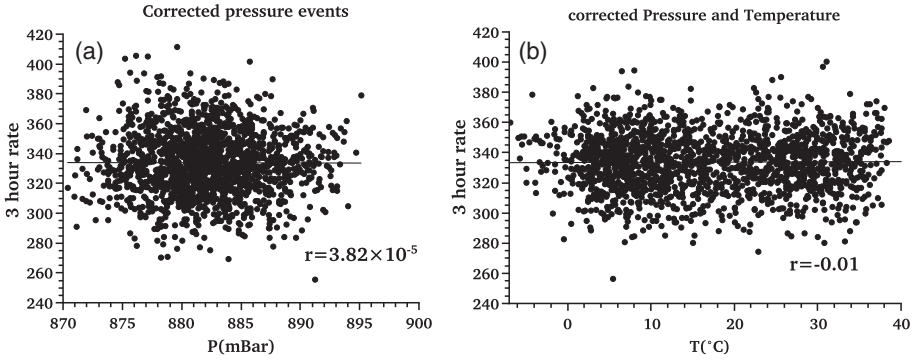

FIG. 4. Corrected 3-h counts after affecting the atmosphere pressure (a), and then affecting the atmosphere temperature (b).

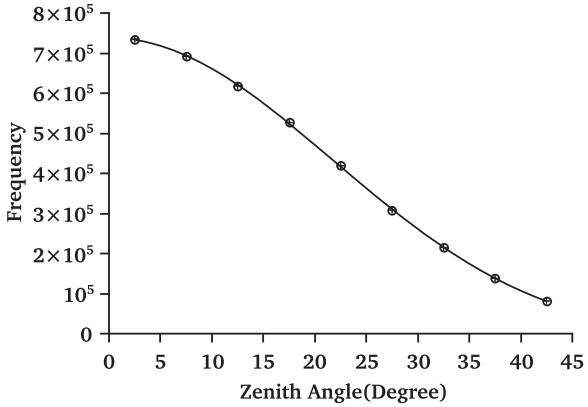

FIG. 5. Zenith angle distribution per solid angle.

several independent physical parameters: (i) the characteristics of the primary cosmic ray which initiates an air shower, e.g., energy and mass of the primary, (ii) the type of the array detectors, (iii) the trigger condition used to detect air showers, (iv) the array layout, (v) the geometry of the incoming shower, e.g., its incidence zenith angle and distance of shower core to the array center [23]. To show these dependencies, the trigger probability function, $P(r, E)$, has been presented as a fraction of showers in the energies of interest (E) which fulfill the trigger condition in different bins of shower core distance from the array center (r), as [24]

$$P(r, E) = \frac{N_{\text{trigger}}(r, E)}{N_{\text{incident}}(r, E)}. \tag{4}$$

Where $N_{\text{trigger}}(r, E)$ and $N_{\text{incident}}(r, E)$ are number of showers with energy E which fulfill the trigger condition at distance r and total number of incident showers with given parameters r and E, respectively.

In addition to the trigger probability function, number of triggered events per day in different bins of energy, $N(E, E + \Delta E)$, can be calculated for different array layouts by a convolution of the trigger probability function $P(r, E)$ and differential flux of primary cosmic rays $\Phi(E)$ (per area, time, solid angle, and energy) as

$$N(E, E + \Delta E) = \int_S \int_E^{E+\Delta E} P(r, E)\Phi(E) dS dE \int d\Omega \int dt. \tag{5}$$

Where the intervals are selected according to the default initial conditions in the simulations. S is the surface of a square grid which considered to study showers arriving inside and outside of the array and trigger it, and $E + \Delta E = 10^{0.5}E$ corresponds to the energy bin widths of 0.5 in logarithmic scale from the simulation. $\Phi(E)$ (Eqs. (6), (7) and (8)) is a primary all-particle spectrum in the *knee* region determined with the Tibet air shower array which is located at an almost ideal atmospheric depth for this energy range and is highly instrumented [25]. In the energy range below the *knee*, for $E < 5.62 \times 10^{14}$ eV,

$$\Phi(E) = 1.5 \times 10^{-20} \left(\frac{E}{5.62 \times 10^{14}}\right)^{-2.60\pm0.04} \times [\text{m}^{-2}\,\text{s}^{-1}\,\text{sr}^{-1}\,\text{eV}^{-1}], \tag{6}$$

and above the *knee*, for $E > 7.08 \times 10^{15}$ eV,

$$\Phi(E) = 1.2 \times 10^{-23} \left(\frac{E}{7.08 \times 10^{15}}\right)^{-3.00\pm0.05} \times [\text{m}^{-2}\,\text{s}^{-1}\,\text{sr}^{-1}\,\text{eV}^{-1}], \tag{7}$$

and in the *knee*, at $E = 1.78 \times 10^{15}$ eV,

$$\Phi(E) = 6.7 \times 10^{-22} [\text{m}^{-2}\,\text{s}^{-1}\,\text{sr}^{-1}\,\text{eV}^{-1}]. \tag{8}$$

3600 extensive air showers with a composition of 88% proton and 12% alpha as primary particles, using the CORSIKA code (version 6.9) have been simulated. QGSJET-II [26] and GHEISHA ($E \leq 80$ GeV) [27] models have been employed for high and low energy hadronic interactions, respectively. At high energies, the showers have been generated in the High Performance Computing Center (HPCC) of Sharif University of Technology with respect to time consuming simulations.

It is worth noting that the cutoff energy of secondary particles kinetic energy in the CORSIKA is chosen 0.3 GeV for hadrons and muons, and 0.003 GeV for electrons and photons, and particles below their energy threshold aren't further tracked. The response of the detectors to secondary particles of showers is calculated by means of GEANT4 detector simulation toolkit [28]. The energy deposition of particles crossing the detectors is computed using simulated air showers which are used as input for detailed GEANT4 simulations. Optical photons, caused by the energy deposition of charged secondary particles in the scintillator, are emitted isotropically and eventually a fraction of photons will reach the photocathode of the PMT. Therefore the output signal of the PMT is proportional to the amount of light reaching the PMT, the photocathode quantum efficiency of $\eta_{QE} \sim 27\%$ for maximum emission of NE102A plastic scintillator in $\lambda_{\text{max}} = 423$ nm and the PMT gain $\text{G} = 140 \times 10^6$. Considering the output signal of the PMT and the anode load resistor and capacitance, the threshold of each detector is considered -200 mV which is correspond to signals of charged particles around 3 MeV. In other words, according to the cut-off energy of secondary particles implemented in the CORSIKA inputs, passage of particles through matter, optical photon processes and PMT response, all charged particles above 3 MeV can be recorded by the detectors in the simulation.

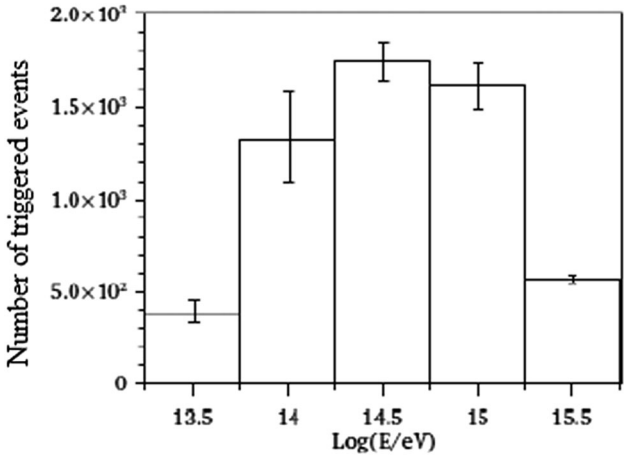

FIG. 6. Energy distribution of triggered events per day for the pentagon array.

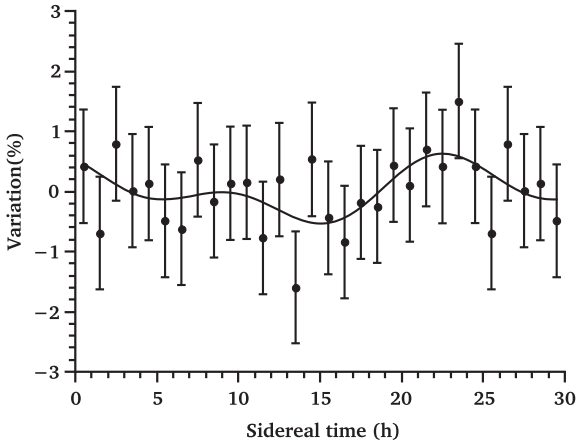

FIG. 7. Variation in the intensity of cosmic rays in terms of sidereal time (points). the black line corresponds to a the first and second harmonic fit to the data.

Air showers were simulated with azimuth angles from 0° to 360° and zenith angles between 0° and 60° distributed as $I \propto \sin\theta\cos\theta\ \mathrm{d}\theta$ (which the *sine* term respects the solid angle element of the sky, while the *cosine* term takes into account the geometrical efficiency of a flat horizontal detector). The energy of primaries is discretely distributed in a range between 10^{12} eV and 10^{16} eV in steps of 0.5 in $\log E$. As mentioned above, cutoff energy of 0.3 GeV and 0.003 GeV are selected for muons and electrons, respectively.

Figure 6 shows the energy distribution of triggered events per day for the pentagon array. It should be noted that the errors are due to systematic uncertainties of the cosmic ray spectrum [Eqs. (6), (7), and (8)] which is used in the Monte Carlo simulations to estimate the number of triggered events. As can be seen, the maximum happens in 3×10^{14} eV, and the sensitive energy range of the array is in the decade below 1 PeV.

D. Anisotropy analysis

The sidereal time (ST) of every event is calculated from $ST = ST_\circ + \alpha(ZT - ZT_0)$. The value ST_0 is available in an almanac [29] for the time ZT_0. ZT is the solar time, and α is a constant with value 1.00273790935. Figure 7 shows the percentage variation in intensity of the cosmic rays in terms of apparent sidereal time. The error bars show the statistical errors only. The data are fitted to a curve with the first and second hamonomics according to Eq. (9),

$$f = A_I \cos\left[\frac{2\pi}{24}(t-\phi_I)\right] + A_{II}\cos\left[\frac{2\pi}{12}(t-\phi_{II})\right]. \quad (9)$$

Where t is in hours. Table I shows the fitting parameters.

However, by correcting the effects of atmospheric pressure and temperature, the 3-h distribution of cosmic rays becomes narrower than its raw state (the vertical width of the curve in Fig. 4(b) relative to Fig. 3), but this narrowed distribution still has a FWHM of about 37/335 ≃ 11%. This width can still have uncorrected contributions to the signal beneath that. As shown in Fig. 7, the coherent anisotropic signal from the depression to the peak is about ≃6%, which is less than the width mentioned above. So to have a credible true sidereal signal, we consider the antisidereal time variation. Since solar seasonal modulation equally influences the amplitudes of the antisidereal and spurious sidereal, the antisidereal distribution acts as a useful indicator for modulation effects. So the data must be scrutinized for such behavior before ascribing any physical significance to the sidereal vector estimated in the experiment. Figures 8 and 9 show the antisidereal and solar distributions respectively, and the fitting parameters are also shown in Table I. As shown in Table I, the first harmonic amplitude of apparent sidereal distribution is almost identical to the antisidereal distribution. This indicates that the sidereal distribution may well not be significantly higher than noise, perhaps as a result of incomplete corrections for all environmental effects. Many experiments consider the relationship of the events rate with the atmospheric temperature at high altitudes (often the level of 100 mb) since this is the location of the early shower interactions. But we do not have information on the layers above ground level and we have only made environmental corrections to this level. The first harmonic

TABLE I. Fitted parameters in Eq. (9).

	A_I (%)	ϕ_I (h)	A_{II} (%)	ϕ_{II} (h)
Apparent Sideral	0.39±0.15	0.15±1.47	0.29±0.15	21.98±0.98
Antisidereal	0.36±0.16	12.32±1.70	0.28±0.16	2.88±1.13
Solar	0.25±0.22	8.98±3.07	0.19±0.21	3.36±2.05

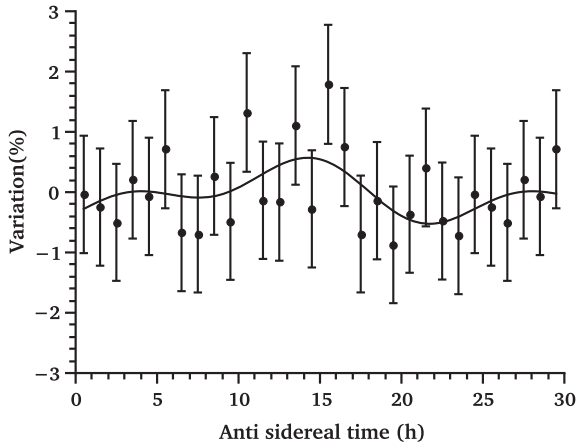

FIG. 8. Variation in the intensity of cosmic rays in terms of anti-sidereal time (points). the black line corresponds to a the first and second harmonic fit to the data.

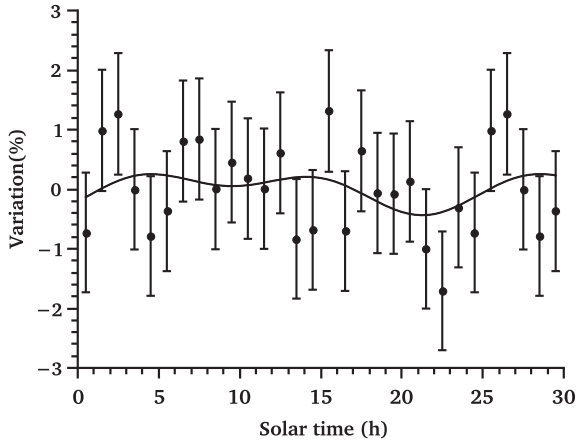

FIG. 9. Variation in the intensity of cosmic rays in terms of solar time (points). the black line corresponds to a the first and second harmonic fit to the data.

amplitude and phase can, therefore, be used to quantify the distortion induced in the sidereal anisotropy [8].

If the amplitude and phase of the first harmonic corresponding the apparent sidereal, antisidereal, and solar times are represented by $(A_{\mathrm{ApS.}}, \phi_{\mathrm{ApS}})$, $(A_{\mathrm{AntS.}}, \phi_{\mathrm{AntS.}})$, and $(A_{\mathrm{Sol.}}, \phi_{\mathrm{Sol.}})$ respectively, using the Farley method [8], the amplitude and phase of the true sidereal, $(A_{\mathrm{TS.}}, \phi_{\mathrm{TS.}})$, is obtained by the following equations:

$$A_{\mathrm{TS.}}^2 = A_{\mathrm{ApS.}}^2 + A_{\mathrm{AntS.}}^2 - 2A_{\mathrm{ApS.}}A_{\mathrm{AntS.}}\cos(\phi_{\mathrm{ApS.}} + \phi_{\mathrm{AntS.}} - 2\phi_{\mathrm{Sol.}}), \quad (10)$$

$$\tan\phi_{\mathrm{TS.}} = \frac{A_{\mathrm{ApS.}}\sin\phi_{\mathrm{ApS.}} - A_{\mathrm{AntS.}}\sin(2\phi_{\mathrm{Sol.}} - \phi_{\mathrm{AntS.}})}{A_{\mathrm{ApS.}}\cos\phi_{\mathrm{ApS.}} - A_{\mathrm{AntS.}}\cos(2\phi_{\mathrm{Sol.}} - \phi_{\mathrm{AntS.}})}. \quad (11)$$

Using Table I, $A_{\mathrm{TS.}} = (0.49 \pm 0.50)\%$, and $\phi_{\mathrm{TS.}} = (21.04 \pm 1.01)$ h are calculated.

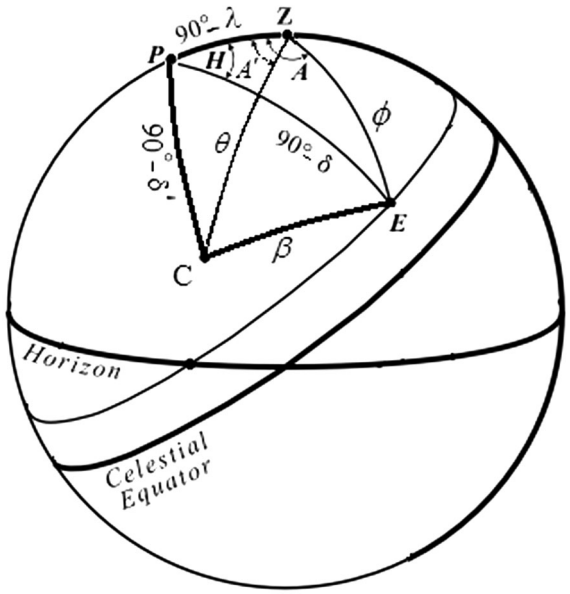

FIG. 10. Celestial coordinate: E = direction of Earth's motion, C = direction of cosmic ray, Z = zenith, P = direction of North pole.

The CGE would contribute to the component A_I in the sidereal time asymmetry. This analysis shows that the anisotropy has a peak close to the true sidereal time 21.04 h, when the zenith is about toward the earth's motion. The amplitude of the first harmonic is 0.49%. So there is a definite sidereal time variation whose phase and amplitude are close to those predicted. To calculate the anisotropy value due to CGE, i.e., the value δ_{CG} in Eq. (1), a mean value for $\cos\beta$ is needed. Assume λ is the latitude of the observer, δ the declination of the direction of Earth's motion, and H the hour angle between the observer's meridian and the direction of motion. Suppose ϕ is the angle between the observer's zenith and the direction of earth's motion. As shown in Fig. 10, $\cos\phi$ is obtained as,

$$\cos\phi = \sin\delta\sin\lambda + \cos\delta\cos\lambda\cos H. \quad (12)$$

On the other hand, $\cos\beta$ (Which β is the angle between the direction of the cosmic ray and the direction of Earth's motion), is calculated by

$$\cos\beta = \cos\phi\cos\theta + \sin\phi\sin\theta\cos\gamma. \quad (13)$$

Where θ is the zenith angle of cosmic ray and γ difference between the azimuthal angle of the direction of Earth's motion and of cosmic ray (Fig. 10), that is $\gamma = A - A'$, which A and A' are obtained by

$$\sin\delta = \sin\lambda\cos\phi + \cos\lambda\sin\phi\cos A, \quad (14)$$

and

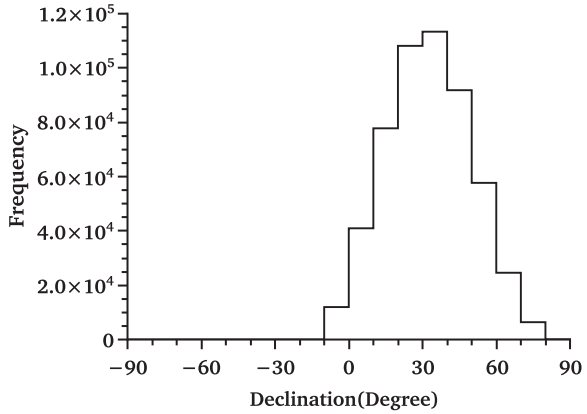

FIG. 11. Distribution of EAS events vs declination angle.

$$\sin\delta' = \sin\lambda\cos\theta + \cos\lambda\sin\theta\cos A'. \quad (15)$$

Where δ' is the declination of cosmic ray. According to Eqs. (12)–(15), the 24-h mean of the projection of cosmic ray along the direction of Earth's motion ($\langle\cos\beta\rangle$) may be obtained. Using $\lambda = 35°43'$ and $\delta = 47°$, we calculated the 24-h mean value of $\langle\cos\phi\rangle \simeq 0.43$ with Eq. (12). With the distribution of $\cos^n\theta\sin\theta d\theta$, with $n = 7.2$, we calculated the mean value of $\cos\theta = 0.91$. The mean value of A was obtained $\simeq 49°$ by using Eq. (14). The mean value of A' was also obtained by using the mean value δ'. Figure 11 shows the distribution of cosmic rays declination. The mean value of declination is $\delta' = 32.5°$, and from Eq. (15), A' obtains $\simeq 90°$. Finally from Eq. (13) a value of 0.68 is obtained for $\cos\beta$ and this is multiplied by the expected CGE amplitude of 0.345% to yield a predicted effect of expected value of 0.24%. The value obtained from experimental data is 0.49% which about 0.25% is more than the CGE value. This remaining asymmetry of 0.25%, presumably has an origin different to the that of the CGE.

Since the recorded data are in Tehran with latitude 35°43′N, the majority of cosmic rays are from the spiral arm inwards direction, which is at about 20 h in right ascension and 35° in declination [30]. So the remaining asymmetry is probably due to unidirectional anisotropy of cosmic ray flow along the Galactic arms. A simple diffusion model [31] suggests that value of this asymmetry, 0.25%, would be roughly equal to the ratio of the scattering mean free path to a characteristic dimension of the containment region (i.e., the central Galactic region, with a scale of 10 kpc). So with amplitude of the anisotropy of 0.25% found in this work, we obtain a mean free path of about 25 pc which is about perhaps 25 times of gyro radius.

Since the anisotropies are low, it is necessary to consider the effect of counting statistics for a finite measured data set. The well-known Rayleigh formula for probability of obtaining fractional amplitude greater than r is given by [32],

$$P(>r) = e^{-k_0}; \qquad k_0 = r^2N/4. \quad (16)$$

Here N is the total number of events used in the data set. k_0 is a convenient and proper parameter for characterizing the anisotropy amplitude probability distribution. The fractional amplitude $\sqrt{2}r_{rms}$ which is equivalent to $k_0 = 1$, as noise amplitude is considered. For the number of events that we have accumulated, 532797, the total amplitude of 0.49% obtained in this work can be arisen by chance with a probability of $P(>r) \sim 4.1\times10^{-2}$ corresponding to $k_0 = 3.2$. This shows a significant anisotropy ($k_0 > 1$) at the sidereal period. So we conclude that this data set gives evidence of anisotropy.

IV. CONCLUSION

An array of detectors including 5 plastic scintillators has been installed at Sharif University of Technology in Tehran to study the anisotropy of cosmic ray distribution. An average of about 0.03 events per second was recorded. The zenith angle of the arrival direction of air showers obeys a $\cos^n\theta$ law with $n = 7.2 \pm 0.1$. Cosmic ray data recorded in our array clearly shows an anisotropy in true sidereal time at energies in the decade below 1 PeV. One part of this anisotropy is due to Earth's motion around the Galaxy (the CGE), but our measured asymmetry suggests the possible existence of some other additional effects, probably a unidirectional anisotropy of cosmic ray flow along the Galactic arms. The first harmonic amplitude of our total measured anisotropy is about 0.49%. The CGE contribution to this anisotropy is about 0.24% and the rest, 0.25%, is predicted to be due to the flow along the Galactic arm. The latter anisotropy suggests a mean free path of about 25 pc for these high-energy cosmic rays. The evidence of these anisotropies is based on the value of the parameter k_0, found in this work to be 3.2, that is, more than $k_0 = 1$, the value for the noise amplitude.

Despite all the predictions mentioned, we intend to continue the experiment for a longer period to reduce the statistical errors.

ACKNOWLEDGMENTS

This research was supported by a grant from office of vice president for science, research and technology of Sharif University of Technology. The authors wish to express their gratitude to Mr Mostafa Heydarzad for all his meritorious helps.

[1] J. W. Armstrong, B. J. Rickett, and S. R. Spangler, Astrophys. J. **443**, 209 (1995).
[2] P. K. F. Grieder, *Extensive Air Showers* (Springer, New York, 2010).
[3] V. S. Ptuskin, Adv. Space Res. **19**, 697 (1997).
[4] A. G. K. Smith and R. W. Clay, Aust. J. Phys. **50**, 827 (1997).
[5] A. H. Compton and I. A. Getting, Phys. Rev. **47**, 817 (1935).
[6] J. Poirier, C. D'Andrea, and M. Dunford, in *Proceeding of 27th ICRC, Hamburg, Germany* (Copernicus Gesellschaft, 2001), p. 3930.
[7] T. F. Lin *et al.*, in *Proceeding of 26th ICRC, Salt Lake city, USA, 1999*, Vol. 2 (American Institute of Physics, Melville, USA, 2000), p. 100.
[8] F. J. M Farley and J. R. Storey, Proc. Phys. Soc. London Sect. A **67**, 996 (1954).
[9] H. Kojima *et al.*, in *Proceeding of 27th ICRC, Hamburg, Germany, 2001*, Vol. 10 (Copernicus Gesellschaft, 2001), p. 3943.
[10] H. Kojima *et al.*, in *Proceeding of 28th ICRC, Tsukuba, Japan, 2003*, Vol. 7 (Universal Academy Press, 2003), p. 3957.
[11] K. Nagashima *et al.*, Nuovo Cimento Soc. Ital. Fis. **12C**, 695 (1989).
[12] K. Nagashima, K. Fujimoto, and R. M. Jacklyn, J. Geophys. Res. **103**, 17429 (1998).
[13] T. Kifune, T. Hara, Y. Hatano, N. Hayashida, M. Honda, K. Kamata, M. Nagano, K. Nishijima, G. Tanahashi, and M. Teshima, J. Phys. G **12**, 129 (1986).
[14] M. Aglietta *et al.*, Astrophys. J **470**, 501 (1996).
[15] K. H. Kampert and A. A. Watson, Eur. Phys. J. H **37**, 359 (2012).
[16] Y. Pezeshkian, M. Bahmanabadi, M. A. Motlagh, and M. Rezaie, Nucl. Instrum. Methods Phys. Res., Sect. A **773**, 117 (2015).
[17] C. L. Bhat, M. L. Sapru, and C. L. Kaul, Nature (London) **288**, 146 (1980).
[18] B. Famoso, P. L. Rocca, and F. Riggi, Phys. Educ. **40**, 461 (2005).
[19] L. I. Dorman, *Cosmic Ray Variations and Space Exploration* (North-Holland, Amsterdam, 1974).
[20] K. Mitsui *et al.*, Nucl. Instrum. Methods Phys. Res., Sect. A **290**, 565 (1990).
[21] S. M. H. Halataei, M. Bahmanabadi, M. K. Ghomi, and J. Samimi, Phys. Rev. D **77**, 083001 (2008).
[22] D. Heck *et al.*, Forschungszentrum Karlsruhe Report No. FZKA6019 (1998).
[23] P. Abreu *et al.*, Astropart. Phys. **35**, 266 (2011).
[24] S. Abdollahi, M. Bahmanabadi, Y. Pezeshkian, and S. M. Moghaddam, Astropart. Phys. **76**, 1 (2016).
[25] M. Amenomori *et al.*, Astrophys. J **461**, 408 (1996).
[26] N. N. Kalmykov, S. S. Ostapchenko, and A. I. Pavlov, Nucl. Phys. B (Proc. Suppl.) **52**, 17 (1997).
[27] H. Fesefeldt, The Simulation of Hadronic Showers: Physics and Applications, Aachen: Physikalische Institute, RWTH (1985). Technische Hochschule.; PITHA.
[28] R. Brun and F. Carminati, GEANT Detector Description and Simulation Tool, CERN Program Library Long Writeup W5013 (1993).
[29] https://www.iiap.res.in/personnel/reks/software/javascript/calclst.php.
[30] R. M. Jacklyn, PASA **6**, 425 (1986).
[31] H. R. Allan, Astrophys. Lett. **12**, 237 (1972).
[32] J. Linsley, Phys. Rev. Lett. **34**, 1530 (1975).